



HAL
open science

New approach in the kinematic $k-2$ source model for generating physical slip velocity functions

J. Ruiz, D. Baumont, P. Bernard, C. Berge-Thierry

► **To cite this version:**

J. Ruiz, D. Baumont, P. Bernard, C. Berge-Thierry. New approach in the kinematic $k-2$ source model for generating physical slip velocity functions. *Geophysical Journal International*, 2007, 171 (2), pp.739-754. 10.1111/j.1365-246X.2007.03503.x . hal-00315602

HAL Id: hal-00315602

<https://hal.science/hal-00315602v1>

Submitted on 5 Jul 2017

HAL is a multi-disciplinary open access archive for the deposit and dissemination of scientific research documents, whether they are published or not. The documents may come from teaching and research institutions in France or abroad, or from public or private research centers.

L'archive ouverte pluridisciplinaire **HAL**, est destinée au dépôt et à la diffusion de documents scientifiques de niveau recherche, publiés ou non, émanant des établissements d'enseignement et de recherche français ou étrangers, des laboratoires publics ou privés.

New approach in the kinematic k^{-2} source model for generating physical slip velocity functions

J. Ruiz,^{1,2} D. Baumont,¹ P. Bernard² and C. Berge-Thierry¹

¹IRSN, Institut de Radioprotection et de Sûreté Nucléaire, France. E-mail: javier.ruiz@irsn.fr

²IPGP, Institut de Physique du Globe de Paris, France

Accepted 2007 May 21. Received 2007 May 18; in original form 2006 June 10

SUMMARY

In an attempt to improve the ground motion modelling, the characteristics of the slip velocity functions (SVF) generated using the kinematic k^{-2} source are investigated and compared to the dynamic solutions proposed in the literature. Several numerical simulations were performed to test the influence of the model parameters on the SVF modelling. Overall, the shapes of SVF are very complex and exhibit a large variability in time and space. However, we found out that the mean SVF is a simple boxcar with duration equal to the largest rise time value. In the areas of weak slip, the SVFs are characterized by the existence of negative values, whereas in large slip areas, the SVF is more impulsive. Overall, on the examples investigated, the SVFs modelled with this k^{-2} source model are different from a typical Kostrov's solution. The critical analysis of the kinematic k^{-2} source led us to identify the Fourier decomposition of the slip to be responsible for these difficulties, and to propose a new recombination scheme. It consists of adding a positive correction to the Fourier slip components. The slip is described as the sum of positive contributions at various scales. The SVFs modelled using this new scheme are greatly improved. Moreover, through several parametrical analyses performed to qualify this new approach, we show that the SVF are corrected while preserving the essential quality of the k^{-2} modelling, that is, the ω^2 spectral shape and C_d apparent directivity of the synthetic accelerograms. Strong ground motion modelling in the near-fault region was made and numerical ground motion parameters were compared to the empirical relationships. We show that predicted peak ground motion is consistent with near-source attenuation laws.

Key words: seismic spectra, source–time functions, strong ground motion, synthetic seismograms.

1 INTRODUCTION

Predicting ground-motion parameters for earthquake scenarios is fundamental for seismic hazard assessment and earthquake design studies. This can be achieved through the development of empirical relationships relating a characteristic of the ground motion with few parameters such as magnitude and site-to-event distance (e.g. Sabetta & Pugliese 1987; Ambraseys *et al.* 1996; Abrahamson & Silva 1997; Boore *et al.* 1997). This strategy remains however difficult to apply in regions of moderate seismicity where strong ground motion data sets are often sparse, especially at short epicentral distances and large magnitudes. In such a case, data recorded in other regions may be added to enlarge the data set (e.g. Berge-Thierry *et al.* 2003). An alternative strategy to predict the ground motion consists to compute synthetic broad-band accelerograms using a seismic source model and a wave propagation numerical scheme (e.g. Berge-Thierry *et al.* 1998; Mai & Beroza 2003). However, natural accelerograms are complex, high-frequency signals which are strongly site-dependent. Indeed, even nearby stations can exhibit

very different spectral and temporal characteristics (e.g. records of the M_w 6.0, 2004 Parkfield event at the stations close to the fault). These complexity and variability in the records are mainly attributed to the high-frequency contents of the source radiation, to the interaction of the wavefield with the complex crustal structure, and to the local site effect response. The challenge of the numerical approach is thus to attempt to model realistic ground motion characteristics (temporal and spectral), irrespectively of the earthquake scenario and source-station configuration considered. This is especially difficult (1) when the target site is located in the vicinity of the extended fault (in such a case the ground motion is strongly controlled by the details of the rupture of the fault area close to the site) and (2) when the site is located in the direction of the rupture propagation (in such a case the ground motion is strongly controlled by the directivity effects).

Several models were proposed to describe the seismic source complexity (e.g. Andrews 1980, 1981; Boore 1983; Papageorgiou & Aki 1983; Bernard & Madariaga 1984; Boatwright 1988; Frankel 1991; Herrero & Bernard 1994; Irikura & Kamae 1994; Zeng *et al.*

1994; Bernard *et al.* 1996; Beresnev & Atkinson 1997). Most of these models use simple slip velocity functions (SVFs) such as box-car, triangular, trapezoidal functions. The case of the k^{-2} source modelling proposed by Bernard *et al.* (1996) is of particular interest because the SVFs strongly vary laterally on the fault (in terms of shape and amplitude). In this model, the slip is decomposed on a Fourier k -spectrum, and each SVF is built by adding each k -contribution with an elementary source–time function with a k -dependent rise time. The resulting SVFs are thus complex, allowing to generate synthetics that simultaneously satisfy a ω^2 spectral model (Aki 1967), with spectral amplitudes scaled to the directivity coefficient at high frequencies. An alternative SVF description which may be more realistic can be provided by dynamic modelling (e.g. Kostrov 1964; Archuleta & Hartzell 1981; Nakamura & Miyatake 2000; Nielsen & Madariaga 2003; Guatteri *et al.* 2004 and Tinti *et al.* 2005) even if this approach is often limited to low frequencies (usually lower than 2 Hz). One may thus attempt to use such a ‘dynamically compatible’ SVF instead of the k -dependent SVFs produced in the k^{-2} source model. However, the source parameters are not independent. Indeed, the spectral characteristics of the ground motion strongly depend on the assumptions made for the slip distribution, rupture and slip velocities (see Andrews 1981; Joyner 1991 or Tsai 1997, for instance). Changing the SVFs without modifying the other source parameters may thus distort the spectral characteristics of the synthetic accelerograms generated by the k^{-2} model, and may not satisfy anymore the ω^2 spectral model.

The aim of this paper is twofold: (1) to characterize the SVFs obtained using the stochastic kinematic k^{-2} source model and compare them with a typical dynamic SVF solutions and (2) to improve the SVF modelling in order to better fit the dynamic SVF solutions proposed in the literature while preserving the spectral radiation of the k^{-2} kinematic model.

2 SVFs OBTAINED FROM DYNAMIC RUPTURE MODELLING

In the early classic dynamic rupture models, Kostrov (1964) derived an analytical SVF solution for a self-similar, circular crack. His solution is singular at the crack tip, and its amplitude falls off as the inverse of the square root of time. This solution has no healing time and thus for convenience, we present a truncated version of the Kostrov’s solution using a rise time value (Fig. 1a). This singularity at the crack tip can be removed by adding a cohesive force (Ida 1972). To solve this more complete dynamic rupture problem, one needs to assume a constitutive law relating the total dynamic traction to the friction law, such as the slip weakening (Andrews 1976) or the rate- and state-dependent (Dieterich 1992) laws. For instance, Nielsen & Madariaga (2003) derive a 2-D, antiplane solution for fixed rupture and healing speeds that satisfies both the wave equation and crack boundary conditions assuming a simple Coulomb friction law in the absence of any rate or state dependence. They obtained an analytical solution for a fundamental fracture mode in the form of a self-similar, self-healing pulse. The analytical SVF obtained is similar to the Kostrov’s (1964) solution but ends at a healing time (Fig. 1b).

The constitutive law and the initial conditions on the fault plane are important since they control the solution. The shape and duration of the resulting SVFs can strongly vary on the fault plane depending on the parameters that were chosen (e.g. Inoue & Miyatake 1998; Nakamura & Miyatake 2000; Guatteri *et al.* 2003). Despite the variability of the SVFs computed in dynamic models, a few attempts were made to define approximate expressions of SVF suitable for use in kinematic strong ground motion modelling (Nakamura & Miyatake 2000; Guatteri *et al.* 2004; Tinti *et al.* 2005). For instance, on the basis of 2-D, and 3-D crack simulations including a slip-weakening friction law, Nakamura & Miyatake (2000) proposed an

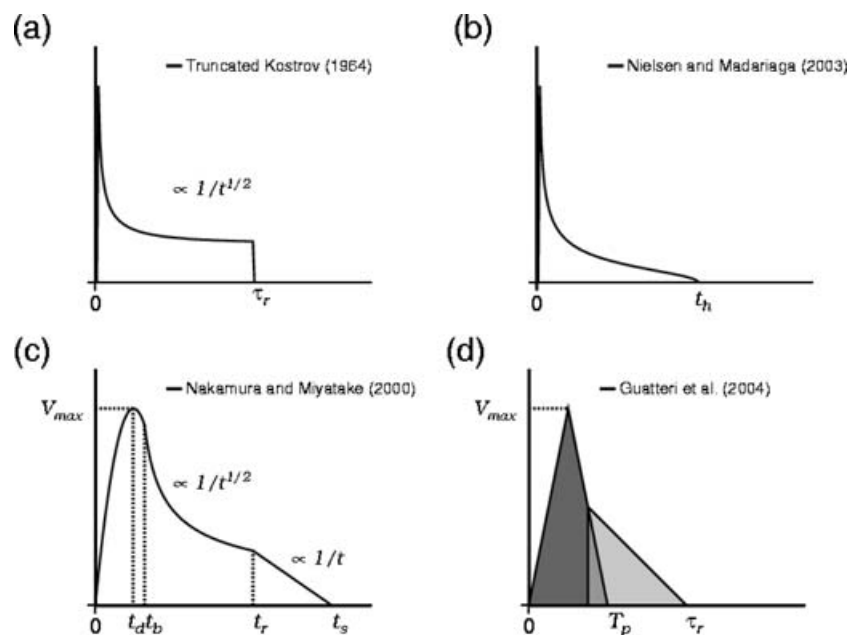


Figure 1. Schematic SVFs derived from dynamic rupture modelling (see text for details). Analytical solutions (a) for a crack proposed by Kostrov (1964) and modified by adding a rise time value and (b) for a self-healing crack proposed by Nielsen and Madariaga (2003). Schematic solutions proposed by (c) Nakamura and Miyatake (2000) and (d) Guatteri *et al.* (2004).

expression of the SVF (Fig. 1c) depending on several parameters mainly related to the stress drop, rupture velocity, critical distance and rigidity values as well as on the dislocation mode. The SVF proposed by these authors is less singular than the analytical solutions previously described. After reaching a maximum slip velocity value, the SVF amplitude decreases as the inverse of the square root of time up to the rise time, then as the inverse of the time up to the healing time. Guatteri *et al.* (2004) proposed another expression, easier to parametrize (Fig. 1d), and characterized mainly by the rise time, the pulse time and the maximum slip velocity value. The latter solution is a schematic version of the Nakamura & Miyatake's (2000) proposition.

3 SVFs OBTAINED FROM k^{-2} KINEMATIC RUPTURE MODELLING

In this section, the SVFs generated by the k^{-2} kinematic model are analysed to define their main characteristics, and are compared with the dynamic modelling solutions.

3.1 The k^{-2} kinematic source model

As we previously noted, several kinematic source models were developed among which stochastic source models (e.g. Andrews 1980; Papageorgiou & Aki 1983; Irikura & Kamae 1994; Herrero & Bernard 1994; Zeng *et al.* 1994; Bernard *et al.* 1996), and pseudo-dynamic models (e.g. Guatteri *et al.* 2003, 2004) that attempt to describe the source complexity. Recent studies proposed different strategies to reproduce the spatial complexity of slip distributions (e.g. Somerville *et al.* 1999; Mai & Beroza 2002; Lavallée & Archuleta 2003). It has been shown (Andrews 1980, 1981) that assuming a slip having a k^{-2} spectral decay in the radial wavenumber domain (Fig. 2), ensures that the radiated displacement spectrum has a standard ω -square spectral shape (Aki 1967) in the far field approximation. It is worth noting that the spectral decay of slip distributions inverted for several events is to the first order in agreement with a k^{-2} spectral decay (Somerville *et al.* 1999; Mai & Beroza 2002). Herrero & Bernard (1994) developed a broad-band, kinematic rupture model based on a self-similar k^{-2} slip distribution. These authors made the working hypothesis of an instantaneous rise time, which resulted in modelling high frequency spectral amplitudes proportional to C_d^2 (C_d being the coefficient of directivity). To better model the high frequency content of the synthetics, Bernard *et al.* (1996) pro-

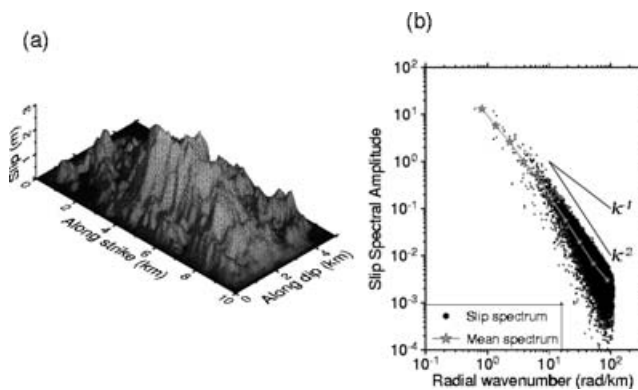


Figure 2. Example of a k^{-2} slip distribution for a magnitude six, earthquake. (a) Spatial and (b) spectral representations in the radial wavenumber. The slip distribution is generated in the Fourier domain with spectral amplitudes proportional to k^{-2} and random phases for $k > k_c$ (k_c cut-off wavenumber).

posed to introduce a propagating pulse and a k -dependent rise time. The elementary source–time function they chose is a boxcar with a k -dependent rise time, $\tau(k)$. This scale-dependent rise time distorts the ω^2 spectrum at high-frequency, allowing the apparent directivity to be equal to C_d . A maximal rise time value is defined (τ_{\max}) equal to L_0/V_r , where L_0 is the width of the slip pulse. This pulse is assumed to propagate at a constant rupture velocity V_r . Bernard *et al.* (1996) and Berge (1997) showed that the characteristics of the radiated spectra depend in particular of the values chosen for V_r/V_s and L_0/L . The k^{-2} kinematic source model proposed by Bernard *et al.* (1996) is attractive because it allows generating realistic broadband accelerograms using heterogeneous slip and rupture process (Berge-Thierry *et al.* 1999; Berge-Thierry *et al.* 2001; Gallović & Brokešová 2004). Furthermore, the synthetics are valid for any distance and fault-station configuration.

3.2 Characteristics of SVFs generated by the k^{-2} model

Following Bernard *et al.* (1996), we can write the SVF as a function of time (t) at a point on the fault (ξ):

$$\Delta \tilde{u}(\xi, t) = \iint \Delta \tilde{u}(k_x, k_y) F[\tau(k_x, k_y), t] e^{ik \cdot \xi} dk_x dk_y. \quad (1)$$

In this equation, $\Delta \tilde{u}$ represents the 2-D Fourier transform of the final slip distribution $\Delta u(x, y)$ on the fault (shown in Fig. 2). The SVFs are computed numerically, by adding each slip Fourier contribution. The elementary source–time function $F[\tau(k), t]$ we used is a boxcar whose duration is k -dependent. In this section, we analyse the SVFs generated by the k^{-2} kinematic model for a magnitude six event, slip distribution ($10 \times 5 \text{ km}^2$, Fig. 2). The shear wave velocity V_s was fixed to 3.7 km s^{-1} . Several combinations of V_r/V_s (0.7, 0.8 and 0.9) and L_0/L (0.05–0.4) were tested. The range of values explored corresponds to the ones already used in the parametrical analysis of previous studies (Bernard *et al.* 1996; Berge 1997). For being concise, only two cases are reported here for two pulse widths (L_0/L) equal to 0.2 (leading to τ_{\max} equal to 0.68 s) and 0.4 ($\tau_{\max} = 1.35$ s), and a constant V_r to V_s ratio equal to 0.8. The parameter τ_{\max} corresponds to a long-wavelength rise time. It affects the wavelengths larger than the pulse width (Bernard *et al.* 1996). These values are compatible with the range of rise-time provided by the kinematic rupture inversion for $M_w \sim 6.0$ events (e.g. Ide 1999; Miyakoshi *et al.* 2000; Tselentis & Zahradnik 2000; Horikawa 2001; Baumont *et al.* 2004 for which rise times vary from 0.1 to 4 s). Fig. 3(a) shows few SVFs that were computed with L_0/L ratio equal to 0.2 ($\tau_{\max} = 0.68$ s). The strongest slip velocity amplitudes are spatially correlated with areas of large slip, the weakest amplitudes being located at the edges of the fault plane where the slip dies away. In this example, the maximum peak-slip velocity peak reaches about 7.5 m s^{-1} , which is high, whereas the mean slip velocity is much lower, being equal to 1.2 m s^{-1} . This high value obtained for the SVF peak amplitude is related to the high stress drop value ($\sim 8.5 \text{ MPa}$) associated to this slip distribution. Moreover, it will be shown later on in this paper that the large peak-slip velocity values are restricted to very small areas, which are beyond the optimal resolution of any source kinematic inversion.

To better examine the shape of the modelled SVFs, slip-unit SVFs were computed and are shown in Fig. 3(b). The modelled SVFs have very complex shapes with no clear tendency, exhibiting a large variability in time and space. Several shapes can nonetheless be identified among which one can notice Kostrov's, boxcar, and ramp-like shapes. In this particular case, negative slip velocity values are obtained locally, in particular at the edges of the fault where the whole

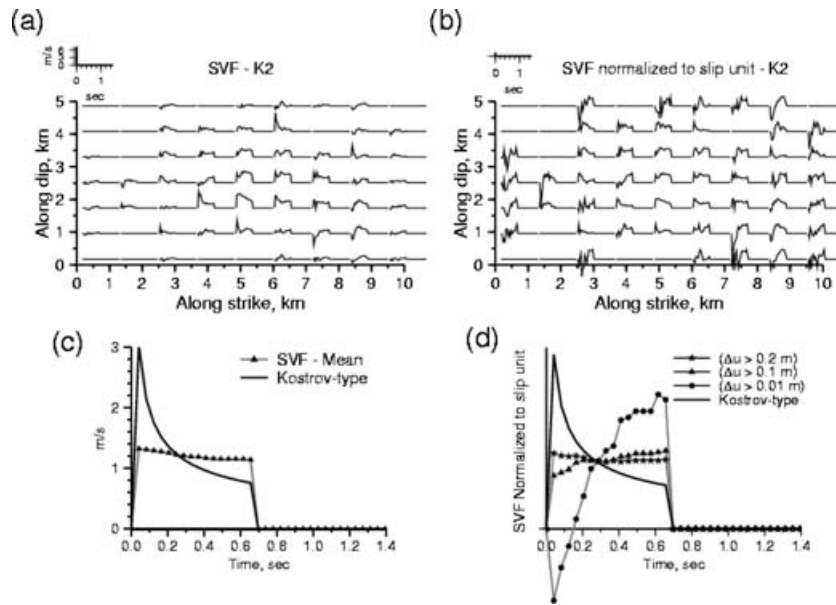


Figure 3. Characterization of the SVFs generated using a k^{-2} source model and assuming $\tau_{\max} = 0.68$ s. (a) Few SVFs computed on the fault plane are shown in absolute amplitudes. To limit the influence of potential numerical noise, SVFs were computed only in the areas where the slip is larger than a threshold value fixed to 0.01 m. (b) Same as (a) except that SVFs were normalized to slip-unit to highlight the variability of the solutions. (c) The mean SVF was estimated from the SVFs obtained at each node of the fault satisfying the threshold criteria. It is compared to the Kostrov-type solution normalized to the equivalent slip value. (d) The mean shape of the SVFs was obtained by averaging the slip-unit SVFs. To test the influence of the weak slip areas, various slip thresholds were considered (values indicated within the parenthesis). These solutions are also compared to a Kostrov-type solution normalized to slip-unit.

solutions are oscillating around zero. For the various combinations of V_r/V_s and L_0/L we explored, the SVFs modelled with the k^{-2} source model are overall different from a typical Kostrov's solution.

To further characterize the SVFs obtained by k^{-2} modelling, we computed numerically the absolute mean SVF (Fig. 3c) by averaging all the solutions computed on the fault plane. The mean solution obtained corresponds roughly to a boxcar function. One can attempt to determine an analytical mean slip velocity in an arbitrary point. Assuming a uniform random phase, one finds:

$$\langle \Delta \dot{u}(\xi, t) \rangle \propto H(t)H(\tau_{\max} - t), \quad (2)$$

where $H(\cdot)$ is the Heaviside function (see Appendix A for details). This analytical expression confirms that the expected mean SVFs is a boxcar function with duration equal to τ_{\max} .

Fig. 3(d) shows the mean shape estimated from the slip-unit SVFs obtained at each node of the fault. A slip threshold criterion was applied to limit the influence of the oscillating SVFs found in the weak slip areas. Various slip thresholds were considered. The solution obtained when most of the fault area is kept in the computation (areas where the slip is greater than 0.01 m) is characterized by a negative value at the beginning followed by an accelerating phase. This solution is obviously controlled by the oscillating SVFs obtained at the edges of the fault. When only areas with a significant amount of slip are included in the computation (slip > 0.1 m), the mean shape of the SVFs corresponds to a boxcar.

Fig. 4 illustrates the effect of τ_{\max} on the proportion of the fault affected by negative slip velocities (for the slip distribution shown in Fig. 2). To this aim, the cumulated negative slip, that is, the amount of slip occurring in the direction opposite to the rake, is computed at each node of the fault by integrating the SVF in the time windows where it takes negative values. For $\tau_{\max} = 0.68$ s, the areas where the SVF has a cumulated negative slip not null remain limited in extension (Fig. 4a), even if locally it can be observed large negative cumulated value. For $\tau_{\max} = 1.35$ s, a large proportion

of the fault is characterized by the presence of a large cumulated negative slip (Fig. 4b) that can locally reach -0.5 m. It can be shown that these areas are correlated with the areas of weak slip. At first glance, these negative slip velocity values could appear to be linked to numerical noise problems but it will be shown in the following section that those inadequate modelling are intimately linked to k^{-2} modelling.

These observations can be generalized to the various combinations of parameters tested. For τ_{\max} values smaller than 0.68 s (corresponding to a narrower slip pulse and/or a larger V_r/V_s value), the proportion of the fault area associated to negative slip velocity values is reduced. For τ_{\max} values larger than 0.68 s, the proportion of the fault area associated to negative slip velocity values increases and the individual SVF shapes are becoming very complex, even if the mean SVF remains close to a boxcar function. In conclusion, whatever the parametric combination tested, the SVF shapes obtained by k^{-2} modelling are not comparable to the solutions derived by dynamic rupture modelling (decaying proportionally to $t^{-1/2}$ when the slip velocity has reached its maximal value).

4 NEW RECOMBINATION SCHEME FOR THE k^{-2} MODEL

4.1 Analysis of the k^{-2} procedure

To understand the origin of the negative SVF values, one should examine in details the procedure followed in the k^{-2} modelling. For simplicity, we grouped the slip 2-D Fourier contributions by successive bands of k (Fig. 5). One can observe that whereas at long wavelength, the slip contribution is strictly positive, at shorter wavelength, the slip contributions can be either positive or negative. Let us recall that each slip contribution to the SVF is set up with a k -dependent rise time that is inversely proportional to k (i.e.

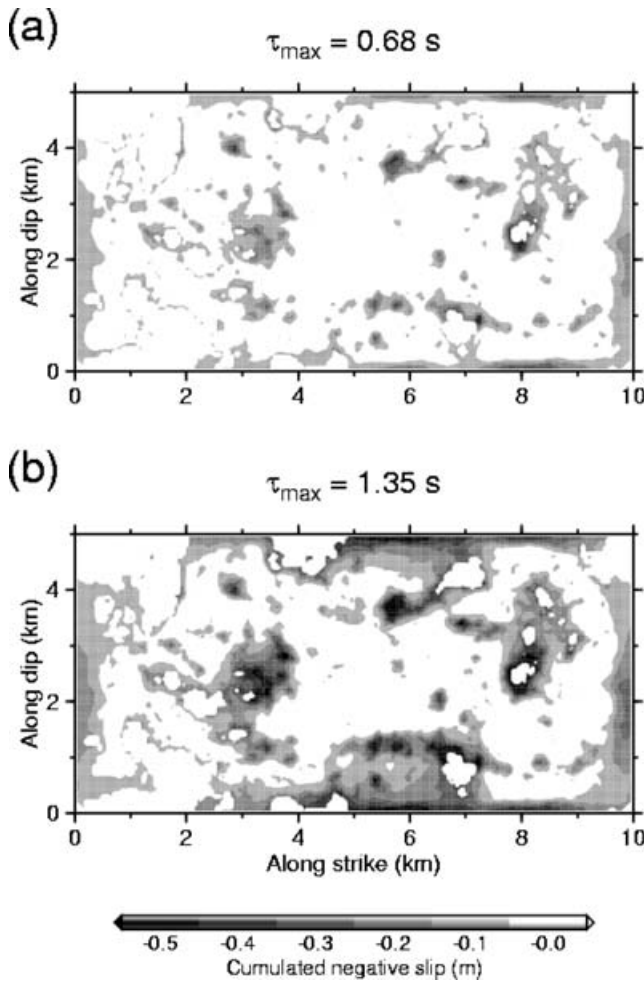


Figure 4. Spatial analysis of the SVF behaviour. Cumulated negative slip computed for each grid node on the fault plane for two rise time values (a) $\tau_{\max} = 0.68$ s and (b) $\tau_{\max} = 1.35$ s. White zones corresponds to strictly positive SVF or slip null.

proportional to the wavelength). Consequently, the negative or positive slip contributions at short wavelength are concentrated over a short rise time at the beginning of the SVFs, resulting in slip velocity amplitudes that can exceed the contributions at long wavelength that are distributed over a larger rise time. The SVFs can thus take punctually significant negative values. Moreover, as shown by Fig. 5, all slip contributions at intermediate to short wavelength oscillate around zero, with a mean value equal to zero. Thus, these slip contributions to the SVF are null when averaged on the fault plane. In other words, only the long wavelength has non zero mean value; equal to the mean slip, which is set up with a constant rise time (τ_{\max}). Hence, the expected mean SVF is a boxcar function of duration equal to the rise time of the long wavelength, in agreement with what we found numerically (Fig. 3c).

4.2 An alternative to the k^{-2} procedure

In order to generate SVFs comparable to the dynamic modelling solutions, we have shown that the short-wavelength slip contributions should be corrected to be mostly positive. This can be achieved by adding a zero order correction to each spectral contribution to the

SVF, which can be written as followed:

$$\Delta \dot{u}_{\text{new}}(\xi, t) = C_n \cdot \left\{ \int \Delta \tilde{u}(k) F[\tau(k), t] e^{ik\xi} dk + \int \Delta u_c(k) F[\tau(k), t] dk \right\}, \quad (3)$$

where $\Delta u_c(k)$ is the slip correction amplitude set up using the k -dependent rise time scaling law. To preserve the seismic moment, the new SVF is renormalized using the initial slip value through a coefficient of renormalization C_n . The slip correction term has to be adjusted as a function of the slip distribution.

Let us first assume that $\Delta u_c(k)$ is proportional to the slip spectral amplitude, and thus proportional to k^{-2} (Fig. 6a):

$$\Delta u_c(k) = p \Delta \tilde{u}(k). \quad (4)$$

Using the slip distribution used previously and $\tau_{\max} = 0.68$ s, we computed the slip velocity correction function (SVCF) associated to the slip correction term. As shown by Fig. 6(b), the SVCF is characterized by a singularity of large amplitude followed by a fast decay, which makes difficult the adjustment of the p -value.

An alternative strategy is based on a more physical approach. The idea is to describe the slip distribution as a summation of positive slip distributions, at different scales, following an approach similar to that of the summation of fractal sets of source sizes (Anderson 1997). We therefore, define a slip correction by band of k , where the bands of k are defined as $B_0 = [0, dk]$, $B_1 =]dk, 2dk]$, $B_2 =]2dk, 4dk]$, \dots , $B_n =]2^n dk, 2^{n+1} dk]$, \dots , $B_m =]2^m dk, k_{\max}]$. For a given band of k , we defined the slip correction, $\Delta u_{c, B_n}$, proportional to the standard deviation of slip, $\sigma_{\text{RMS}}[\Delta u_{B_n}(\xi)]$, where $\Delta u_{B_n}(\xi)$ is the slip contribution for the band B_n :

$$\Delta u_{c, B_n} = p \sigma_{\text{RMS}}[\Delta u_{B_n}(\xi)]. \quad (5)$$

Thus, depending on p , only some fraction of the bandpassed slip has a negative value. It can be demonstrated that the RMS of the slip corresponding to the band B_n is proportional to k^{-1} at intermediate to short wavelengths (see Appendix A for details), which is illustrated on Fig. 6(a). In order to smooth the correction term effect, the slip correction amplitude is distributed over the band of k (eq. 5), and set up with a k -dependent rise time. Since B_n includes 2^{2n} discrete k -value, the individual correction can be written:

$$\Delta u_c(k) = \frac{\Delta u_{c, B_n}}{2^{2n}}. \quad (6)$$

This correction is constant over the band, but is discontinuous between two adjacent bands. Since the correction amplitude varies on average with a k^{-3} trend (see Appendix A for details), we prefer to distribute the correction in a more continuous way by defining it as followed:

$$\Delta u_c(k) = p C \sigma_{\text{RMS}}[\Delta u_{B_n}(\xi)] k^{-3}, \quad (7)$$

where C is equal to Σk^{-3} in B_n . This alternative expression for the slip correction is plotted in Fig. 6(a). The resulting SVCF shown in Fig. 6(b) is characterized by a decay which is less abrupt than when obtained using a correction term proportional to k^{-2} . To even further minimize the correction, a specific procedure was defined for B_0 . Indeed, for this band, it is not necessary to add its RMS value to obtain only positive slip contribution, so that we choose to fix the correction to the smallest requested amplitude.

In summary, we have seen that the SVCF is constant over the fault plane and is scaled in amplitude by the p factor. Its shape is controlled by the relationship between $\Delta u_c(k)$ and the k^{-1} rise time scaling law. Fig. 7 shows our favourite k^{-3} SVCF calculated for several p and

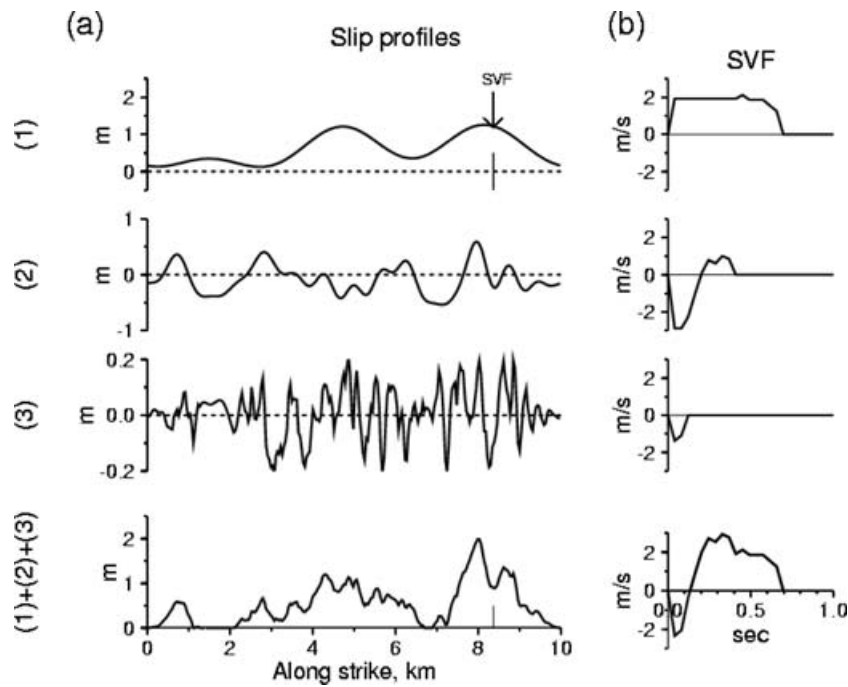


Figure 5. Decomposition of the slip contributions to the SVF modelled with the standard k^{-2} model. Contributions are summed up by band of k to obtain (a) the final slip and (b) the SVF at a given location on the fault plane indicated by the arrow (along-strike = 8.4 km, along-dip = 0.96 km) assuming $\tau_{\max} = 0.68$ s. The bands are defined as follows: (1) $[0-2dk]$, (2) $[3dk-4dk]$, and (3) $[5dk-k_{\max}]$ being the dk value equal to $dk = 2\pi/L = 0.62$ rad km^{-1} .

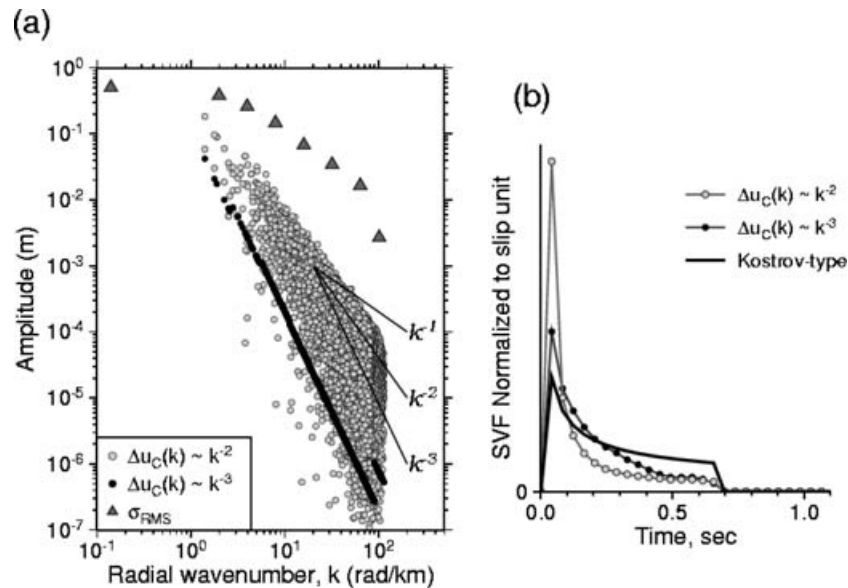


Figure 6. (a) Spectral and (b) temporal characteristics of the slip velocity correction function (SVCF). Several corrections were tested: (1) the amplitude corrections were scaled on slip distribution (light grey circles), that is, proportional to k^{-2} , (2) the amplitude corrections were scaled on the standard deviation of slip defined for each band of k (triangles). To smooth the SVCF, the later correction was distributed over the band following a k^{-3} trend (black circles). (b) The SVCFs are compared to the truncated SVF Kostrov-type solution.

rise time values. For $\tau_{\max} = 0.68$, SVCF peak amplitudes are equal to about 11.2, 8.4, 5.6 and 2.8 m s^{-1} for $p = 2.0, 1.5, 1.0$, and 0.5, respectively. SVCF peak amplitudes remain almost unchanged for $\tau_{\max} = 1.35$ s. Compared to the 7.5 m s^{-1} peak amplitude of the SVF generated using the standard k^{-2} procedure (see Fig. 3), the SVCF peak amplitudes become larger than the uncorrected SVF peak amplitude for p greater than 1.5. Peak amplitudes of the SVCF

can be reduced by about 20 per cent by fixing the correction of B_0 to zero, which will be the case in the following tests.

4.3 Characteristics of corrected SVFs

In this section, we propose to analyse the characteristics of the corrected SVFs obtained with the new k^{-2} recombination scheme

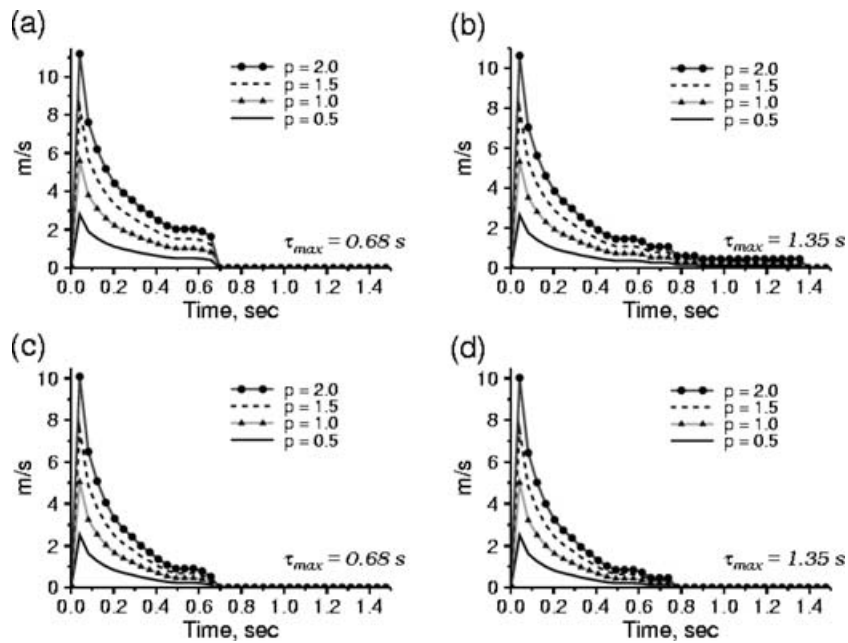


Figure 7. SVCFs computed with the new recombination scheme using several p scaling factor ($p = 0.5, 1, 1.5$ and 2) and assuming $\Delta u_c(k)$ is proportional to k^{-3} . Two maximum rise time values were considered (a) $\tau_{max} = 0.68$ s and (b) $\tau_{max} = 1.35$ s. (b) and (d) Same legend as (a) and (b) except that the contribution of the first band to the SVCF was ignored.

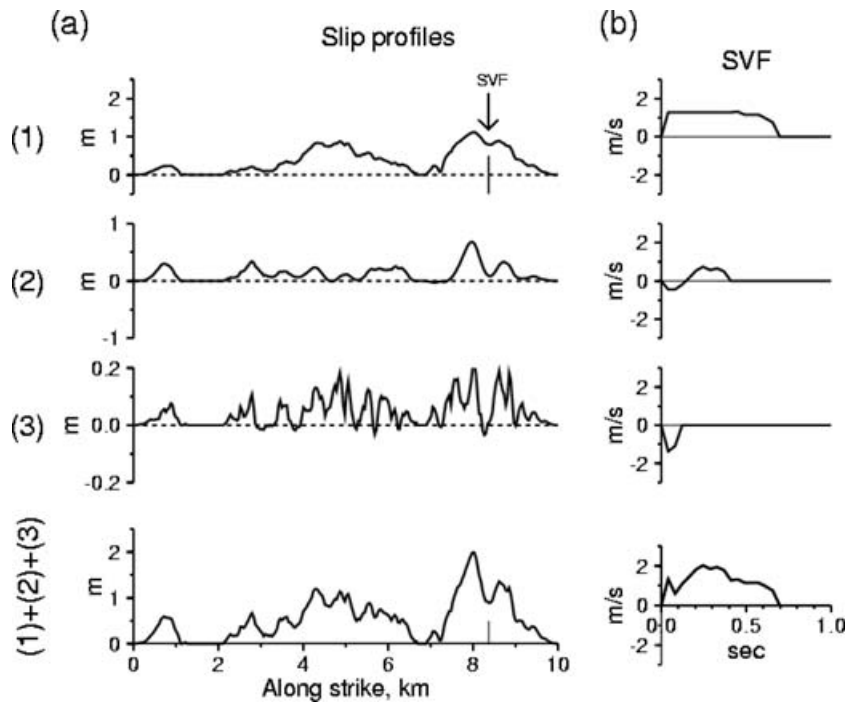


Figure 8. Same legend as Fig. 5 for the new recombination scheme. Whereas the final slip remains unchanged, the SVF obtained is very different from the one obtained using the standard k^{-2} model.

described above. It is important to note that in this new approach, whereas the final slip distribution remains unchanged (Fig. 8), the slip is decomposed in a different way among the various bands of k with respect to the standard k^{-2} modelling (Fig. 5). In particular, short and intermediate wavelengths are all described as mostly positive heterogeneities, which will be added onto the long wavelengths. These contributions are set up with a rise time proportional to the wavelength. The short wavelength contributions to the SVF

will sum up constructively at the slipping phase, which will lead to the development of a singularity of the SVF.

Assuming various p scaling factor ($p = 0.5, 1.0, 1.5$ and 2.0) and $\tau_{max} = 0.68$ s, we modelled a few SVFs on the fault plane. Fig. 9 shows the solutions obtained for p equal to 1, which should be compared to those shown in Fig. 3. On this example, we can notice that the corrected SVFs are almost strictly positive. The correction amplitude is in proportion more important in weak slip areas than

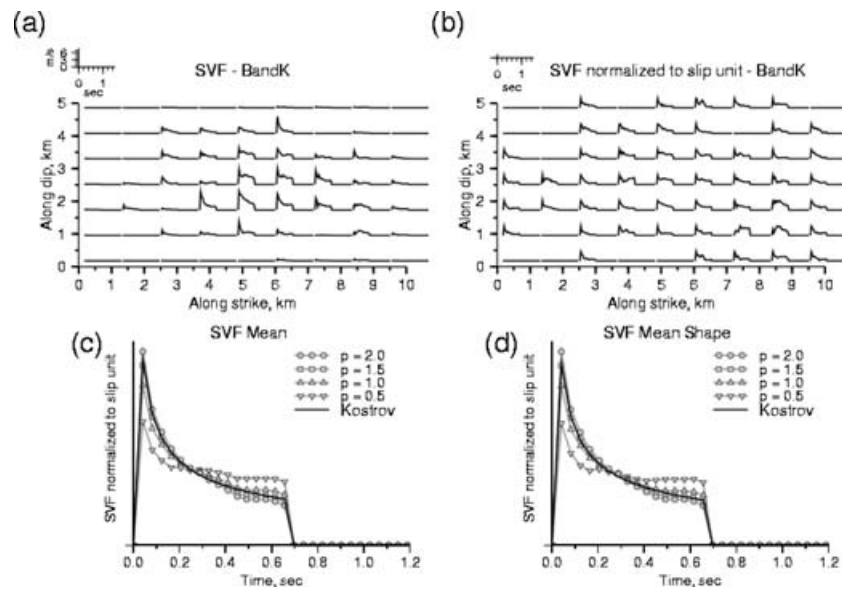


Figure 9. Characterization of SVFs modelled using the new recombination scheme. The slip threshold was fixed to 0.01 m (see Fig. 3), and τ_{\max} to 0.68 s. (a) Few SVFs computed on the fault plane assuming a p scaling factor equal to 1 are shown in absolute amplitudes in m s^{-1} , (b) Same as (a) except that SVFs were normalized to slip unit to highlight the variability of the solutions. (c) The mean SVF is compared to the Kostrov-type solution for various p scaling factors. All the functions were normalized to slip-unit. (d) Same as (c) for the mean shape SVF.

in large slip areas for which the k^{-2} contribution remains important. The peak-velocity varies strongly throughout the fault plane. The maximum peak amplitude of the corrected SVFs reaches about 8.0 m s^{-1} , which represents an increase of 6 per cent relative to the 7.5 m s^{-1} value obtained with the standard k^{-2} model. These high values are located on areas related to the maximum slip. The shape of the corrected SVF varies in space and time, but less strongly than for the standard k^{-2} modelling. Moreover, as illustrated by Fig. 9(c), for p greater than 0.5, both the mean SVF and the mean shape are comparable to the truncated Kostrov's (1964) solution (normalized to the same slip value). Let us recall that at this stage each wavenumber contribution to the final SVF is synchronous with the rupture time arrival and no attempt to remove the singularity was made. The choice of the p -value depends of the τ_{\max} value. For instance, the minimal p -value should be fixed to 1 for τ_{\max} equal to 1.35 s.

5 EFFECTS ON FAR-FIELD ACCELEROGRAMS OF THE CORRECTION SCALING FACTOR

In this section, we aim to qualify the effects of the SVF correction on the temporal and spectral characteristics of accelerograms modelled at large distance. Naturally, the final choice of the p factor value will be guided by the need of correcting the SVFs and at the same time preserving the quality of the k^{-2} modelling. The scenarios we chose to model correspond to a strike-slip event rupturing a vertical fault plane. The rupture front propagates unilaterally. The modelling was performed for three sites located at 100 km from the origin, in directive, non-directive and antidirective azimuths (being $\theta = 0^\circ, 90^\circ$ and 180° in relation to the strike and rupture direction). This simplified source-station geometry was retained to compare the results with the well-known analytical spectral solution. Moreover, let us recall that this source-station configuration is the most critical in strong motion simulation, particularly in the forward rupture direction. The Green's functions were calculated using the analytical solution for the far-field approximation (Aki & Richards 1980), modelling only

S waves in an infinite homogeneous space. For simplicity, the focal mechanism, and the intrinsic attenuation were not included. Synthetic seismograms are obtained by convolving the SVFs with the Green's functions obtained at each fault point.

5.1 Analysis of the S , far-field mean spectra

Mean acceleration spectra are computed for a magnitude six, moderate size event ($L \times W = 10 \times 5 \text{ km}^2$) considering 40 stochastic slip realizations, and the results are compared to the analytical solution for the k^{-2} modelling derived by Bernard *et al.* (1996). However, an adjustment must be made to the proposed analytical solution. Indeed, Fig. 10 shows the mean slip spectrum computed on all slip realizations. The mean slip spectrum clearly follows a k^{-2} slope at high frequency, but one can notice that it does not follow our target spectral shape for which the analytical solution has been developed. As discussed by Galovic (2002), this difference is due to the slip generation procedure which includes edge tapering and zero watering, two treatments that distort the slip spectral shape. Further work will be needed to improve this aspect. Nonetheless, one may consider that the mean slip spectrum has an apparent k_c lower than the theoretical one ($\lambda_c = 8.5$ not 5 km). The analytical spectra will thus be drawn using the apparent k_c value we inferred.

The fault plane was subdivided onto a 256×128 regular grid (mesh size $40 \times 40 \text{ m}^2$). Synthetic seismograms are modelled up to 12 Hz assuming various pulse widths ($L_0 = 0.05L, 0.1L, 0.2L$ and $0.4L$), rupture velocities ($V_r = 0.7V_s, 0.8V_s$ and $0.9V_s$), and p scaling factors ($p = 0.0, 0.5, 1.0, 1.5$ and 2.0). Fig. 11 shows the results obtained at the three stations for $V_r = 0.8V_s$ and $\tau_{\max} = 0.68$ s. For these parameters, the analytical solution has an apparent corner frequency equal to $f_a = C_d V_r / L = 1.5, 0.3$ and 0.17 Hz for the directive, non-directive, and antidirective stations, respectively, and a pulse frequency equal to $f_p = V_r / L_0 = 1.5$ Hz.

Fig. 11(a) shows the mean spectra of accelerograms computed at the three stations using the standard k^{-2} modelling. The results are overall similar to the analytical solution. However, we observe that

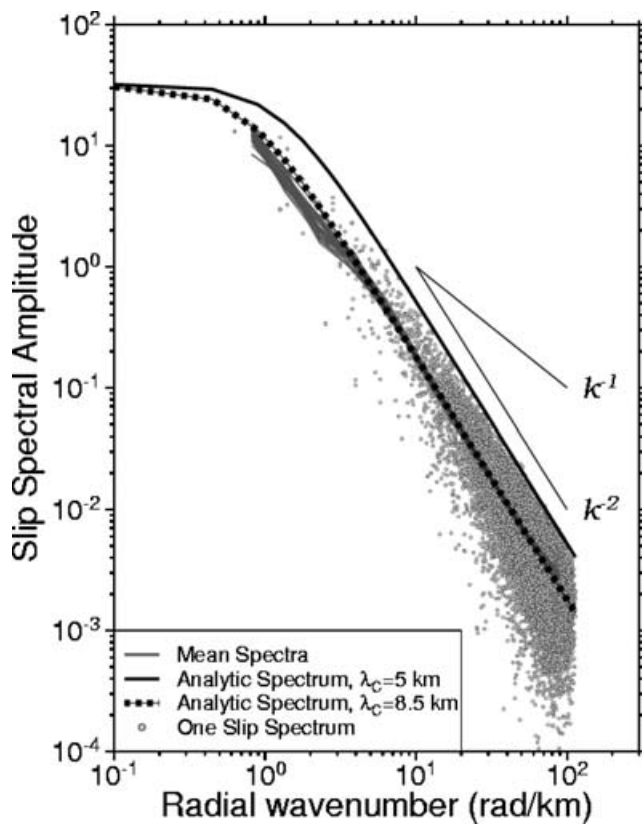


Figure 10. Spectral characteristics of the k^{-2} slip distributions. A set of 40 stochastic k^{-2} slip distributions was generated in the Fourier domain following a spectral target, $\Delta\tilde{u}(k) \sim (1 + (k/k_c)^2)^{-1}$ and $k_c = 2\pi/\lambda_c$, with a cut-off wavelength λ_c equal to 5 km. A water level was applied on each slip distribution as well as a tapering window to smoothen the edge of the slip. The mean slip amplitude spectrum (grey thin lines) is estimated from its discrete Fourier spectrum (grey circles). The mean spectra does not follow the spectral target estimated with $\lambda_c = 5$ km, but rather well follows the one calculated with $\lambda_c = 8.5$ km.

the spectral amplitudes are smaller than the predictions within the frequency range 2–7 Hz for the directive station, 0.3–1 Hz for the non-directive one, and 0.2–0.7 Hz for the antidirective one. These frequency ranges all correspond to the slip contributions for k within 0.8 to 3 rad km $^{-1}$, where statistically the slip spectral amplitudes appear to be slightly weaker than the target slip amplitude (Fig. 3b).

The mean spectra of accelerograms computed with the new recombination scheme using various p scaling factor are shown in Fig. 11(b)–(d) ($p = 0.5, 1.0$ and 1.5 , respectively). We observe that adding a correction to the SVF modelling acts as a filter on the spectra at high frequency. What happens is that in our corrected model, the slip velocity pulse has two components: a spatially variable term, linked to the standard k^{-2} model, and a homogeneous term related to the slip correction. The latter does not contribute to the high frequency spectrum anymore, as it does not fluctuate when the slip velocity pulse propagates along the fault. It does however contribute to the low frequency level. Thus this filtering effect is increasing with p , as seen on the Fig. 11(b)–(d).

In this example, the mean spectral amplitudes obtained for p equal to 0.5 and 1.0 are slightly filtered in particular for the directive and non-directive stations. Moreover, it should be noted that the deficient part of the spectra has been filled up by the corrective term added to the SVFs. The modelled mean spectra follow a ω^2 spectral model with a high-frequency plateau proportional to C_d .

It should also be pointed out that the spectral hole related to the pulse frequency, which is present on the analytical solution for the directive station, has been removed. This results from the fact that the radiation is dominated on average by the mean SVF, which is for the band of k methodology a Kostrov's (1964) like SVF (Fig. 9c), whereas in the analytical solution corresponding to the k^{-2} standard modelling, it is a boxcar function (Fig. 3b). For $p = 1.5$ (Fig. 11d), the mean spectrum for the antidirective station is not flat anymore. The correction effects are becoming too large to preserve the characteristics of the k^{-2} modelling.

Two alternative strategies were also tested. Several studies were conducted to attempt to propose SVF compatible with dynamic modelling that could be used to model the ground motion. Fig. 11(e) shows the mean spectra of synthetics generated using k^{-2} slip distributions with a constant Kostrov's (1964) SVF truncated to a constant rise time, τ_{\max} , that is to say a k -independent SVF. Whereas the mean acceleration spectrum for the directive station still follows a ω^2 spectral model within the range of frequency chosen, the results obtained for the other two stations are strongly filtered. It is clear that directly injecting SVF compatible with dynamic modelling is not sufficient to preserve the spectral characteristics of the synthetic accelerograms (flat acceleration spectrum at high-frequency). The spatial- and temporal-variability on SVFs must be introduced in modelling to simulate ground motions following a ω^2 spectral model. On the other hand, one can try to apply directly a post-processing on the negative values of SVF by applying a water level and renormalizing to the local slip the SVF. Fig. 11f shows that the distortions introduced on the spectra are minor for all stations.

5.2 Analysis of the S, far-field accelerograms

Far-field accelerograms were computed up to 25 Hz for a magnitude 6.5 event ($L \times W = 15 \times 7.5$ km 2). The fault plane was subdivided onto a 512×256 regular grid mesh of about 30×30 m 2 . For convenience, synthetics were shifted by 20 s from origin time. Synthetics are computed for the directive, antidirective and non-directive stations.

Fig. 12 shows the acceleration, velocity and displacement time-series as well as their spectra computed with the standard k^{-2} model and the new recombination scheme. In this example, we assumed a maximum rise time τ_{\max} equal to 1 s, which correspond to a pulse width of 3 km for a rupture velocity equal to 3 km s $^{-1}$. The p scaling factor was fixed to 1. Let us first examine the synthetics computed with the standard k^{-2} model (Fig. 12a, c and e). The synthetic accelerograms are complex, exhibiting a rich-frequency content. The duration and amplitude of the signal are obviously controlled by the location of the stations with respect to the fault. At first glance, the accelerograms obtained are overall of good quality in term of low numerical noise, ω^2 spectral shapes, and C_d apparent directivity. It should be pointed out that, similarly to the results we obtained for the characterization of the far-field mean spectra, the spectral amplitudes follow rather well the analytical spectral solution at all stations, except at intermediate-frequencies at the directive station. The PGA reaches 3.4, 0.61 and 0.17 m s $^{-2}$ for the directive, non-directive and antidirective station, respectively. The PGA obtained at the directive station is large compared to the predictions made by empirical PGA attenuation relationships (e.g. mean PGA $\pm \sigma = 0.15$ – 0.58 m s $^{-2}$ after Berge-Thierry *et al.* 2003), whereas the PGA values obtained at the other two stations are in good agreement with the empirical predictions. Fig. 12(c) and (e) shows the time-series in velocity and displacement (computed with the standard k^{-2}

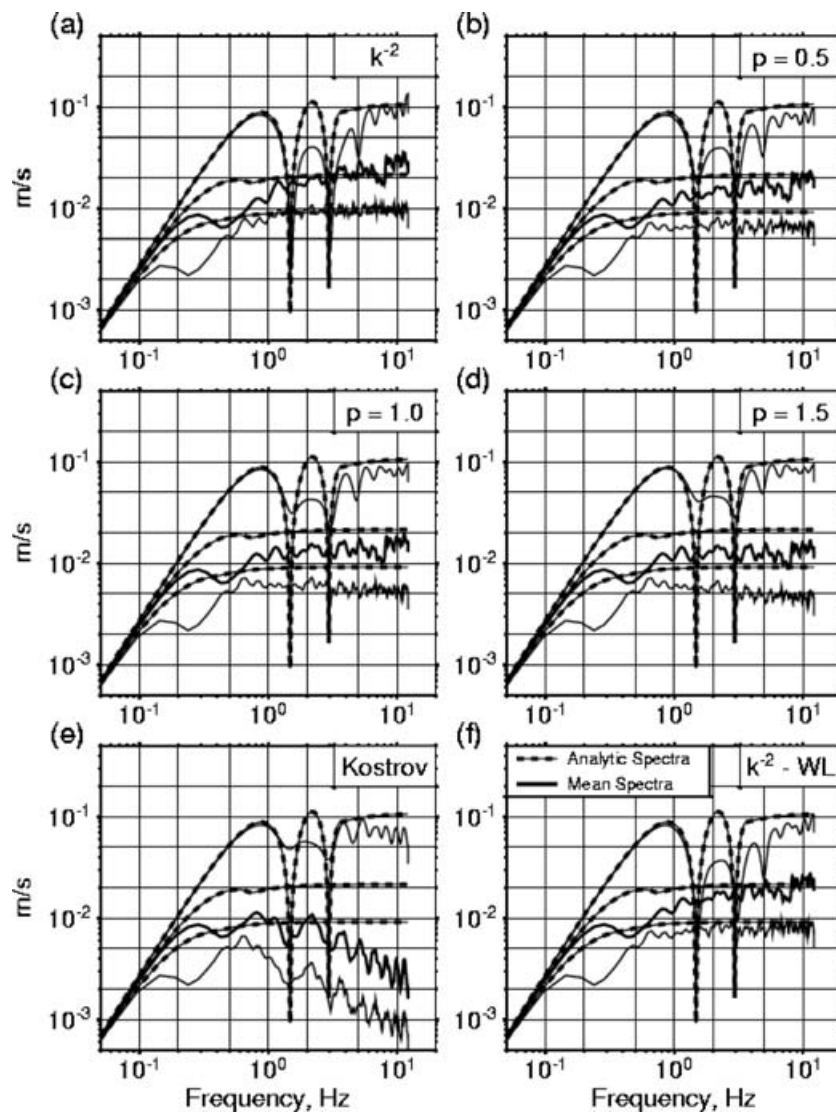


Figure 11. Mean S -wave acceleration spectra computed for the three stations using $\tau_{\max} = 0.68$ s (thin lines). The largest amplitudes spectra are obtained at the directive station, the weakest ones correspond to results at the antirective station, and the intermediate ones to the non-directive station. Several methodologies were tested: (a) standard k^{-2} model, (b–d) new recombination scheme for various p scaling factor (0.5, 1.0 and 1.5, respectively), (e) k^{-2} model set up with a k -independent Kostrov-type SVF truncated to τ_{\max} and (f) k^{-2} model in which a water level was applied on the SVFs. All the solutions are compared to the analytical solution developed for the standard k^{-2} model (dashed line).

model), which naturally have a lower frequency content. One can note, especially for the antirective station, that the starting values of the signal are negative. This is unsatisfactory because we did not include the focal mechanism, and thus the expected displacement time-series are exclusively positive. This negative start is due to the characteristics of the SVF estimated in the areas of weak slip, for which we recall here that SVFs exhibit negative values.

Fig. 12(b), (d) and (f) show the synthetics obtained with the new recombination scheme. The spectral amplitudes of the synthetics satisfy the ω^2 spectral shape, and remain very close to the analytical solution developed by Bernard *et al.* (1996) for the k^{-2} model, even if they were slightly filtered at high frequency. Overall, it can be observed that the amplitudes of the accelerograms have been reduced. In particular, the PGA is about 30–40 per cent smaller (2.3, 0.36 and 0.10 m s^{-2}) than the one obtained with the standard k^{-2} approach. The synthetics computed in displacement and in velocity are overall very similar, except that the beginning and ending signals are bet-

ter modelled with the recombination scheme. We also note that the spectral holes at f_p have disappeared in the new scheme.

Fig. 13 shows the results of a simulation made with a larger rise time ($\tau_{\max} = 2$ s), which corresponds to a 6 km pulse width for a 3 km s^{-1} rupture velocity. The p scaling factor value was not changed ($p = 1$). As the accelerations are controlled by the high-frequency content of the source, that is, the small-scale heterogeneities in our model, the amplitudes of the accelerograms are weakly affected by the change of τ_{\max} for both the standard and new k^{-2} modelling. The most striking difference can be noted on the time-series in displacement (Fig. 13e and f). Indeed, the signal modelled using the new recombination scheme is much more impulsive for the directive station than the one obtained with the standard methodology. The peak ground displacement (PGD) is increased by 50 per cent for the directive station whereas it remains almost the same for the other two stations. The peak ground velocities (PGV) estimated on the time-series generated with the new approach are larger for the

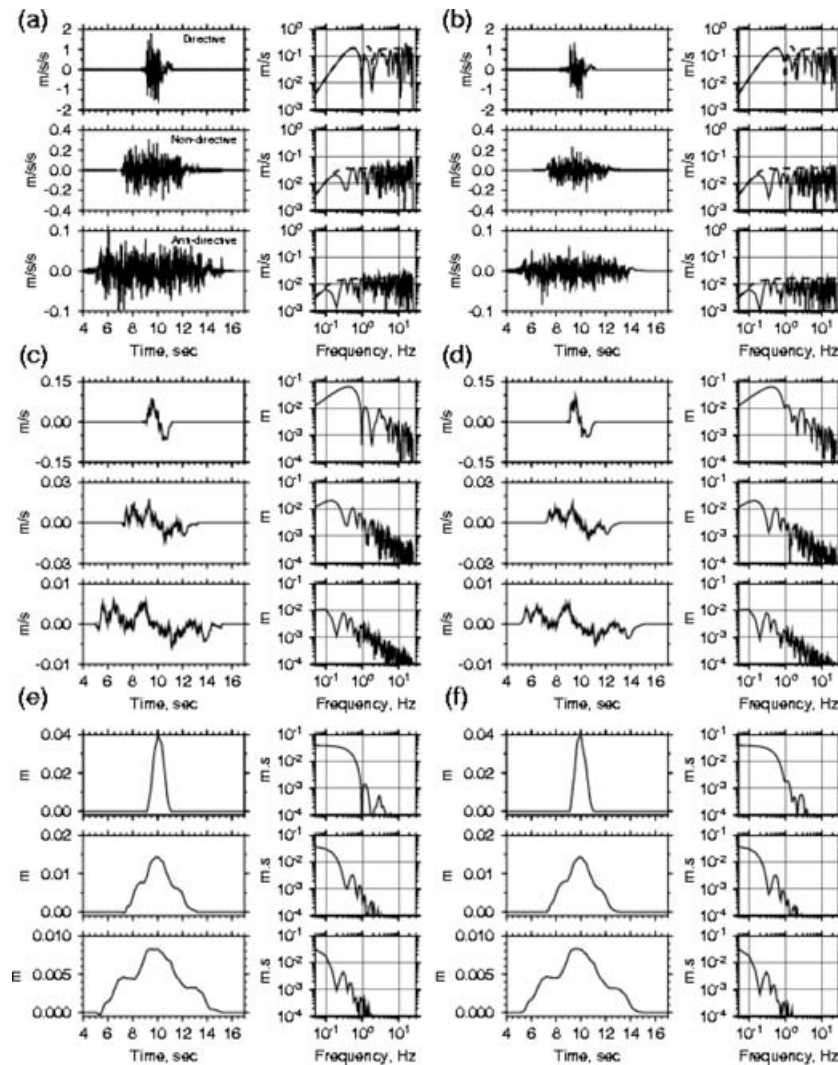


Figure 12. Far-field S wave, synthetics modelled assuming τ_{\max} is equal to 1 s. Both time-series and spectral amplitudes are shown. (a) Acceleration, (c) velocity and (e) displacement ground motion modelled using the standard k^{-2} model. (b) Acceleration, (d) velocity and (f) displacement ground motion obtained with the new recombination scheme assuming a p scaling factor equal to 1. The corresponding directive, non- and antirective stations are labelled in time-series box.

directive station (15 per cent), but smaller for the other stations by about 28 per cent.

The differences observed between the synthetics generated using the two approaches are larger for the displacement, than for the velocity or the acceleration. This can be explained by the fact that the far-field accelerograms are controlled by the second derivative of the SVF, whereas the displacement waveforms are controlled by the SVF itself. Consequently, even if the SVF modelled with these two methods are significantly different, the second derivative of the SVF remains similar and is mostly controlled by the k^{-2} modelling, and not by the added correction. This suggests that the dynamically compatible SVF proposed by the dynamic modelling studies are not sufficient to improve the acceleration modelling, and that additional constraints should also be added on the SVF derivatives. Further work could be done considering for instance the results proposed by Ohnaka & Yamashita (1989) who provided theoretical relationships that characterize the maximum slip velocity value, V_{\max} , and also the maximum slip acceleration for a shear crack as a function of the peak shear stress, the crack velocity and the shear modulus. On the other hand, the large spatial variability of V_{\max} that is required to

satisfy to the ω^2 spectral model using the k^{-2} kinematic modelling may be linked to spatial fluctuations of dynamic parameters. Fig. 14 shows the spatial distribution of V_{\max} on the fault plane obtained with the band of k approach. We observe a large variability reaching strongest amplitudes between 10 and 12 m s^{-1} concentrated in a few patches. The V_{\max} spectrum is shown in the same figure being in average the amplitudes proportional to k^{-1} and $\sim k^{-1.5}$ at low- and high-wavenumber.

6 EFFECTS ON NEAR-FAULT REGION OF STRONG MOTION SIMULATIONS OF THE NEW SVF MODELLED

In the previous section, we analysed the behaviour of the source model in the far-field approximation. In this section, we aim to characterize the ground motion variability produced by our kinematic model in the vicinity of the fault, a region where the strong ground motion predictions are very sensitive to the spatial fluctuations of the SVFs and to the near- and intermediate-field terms. Through this

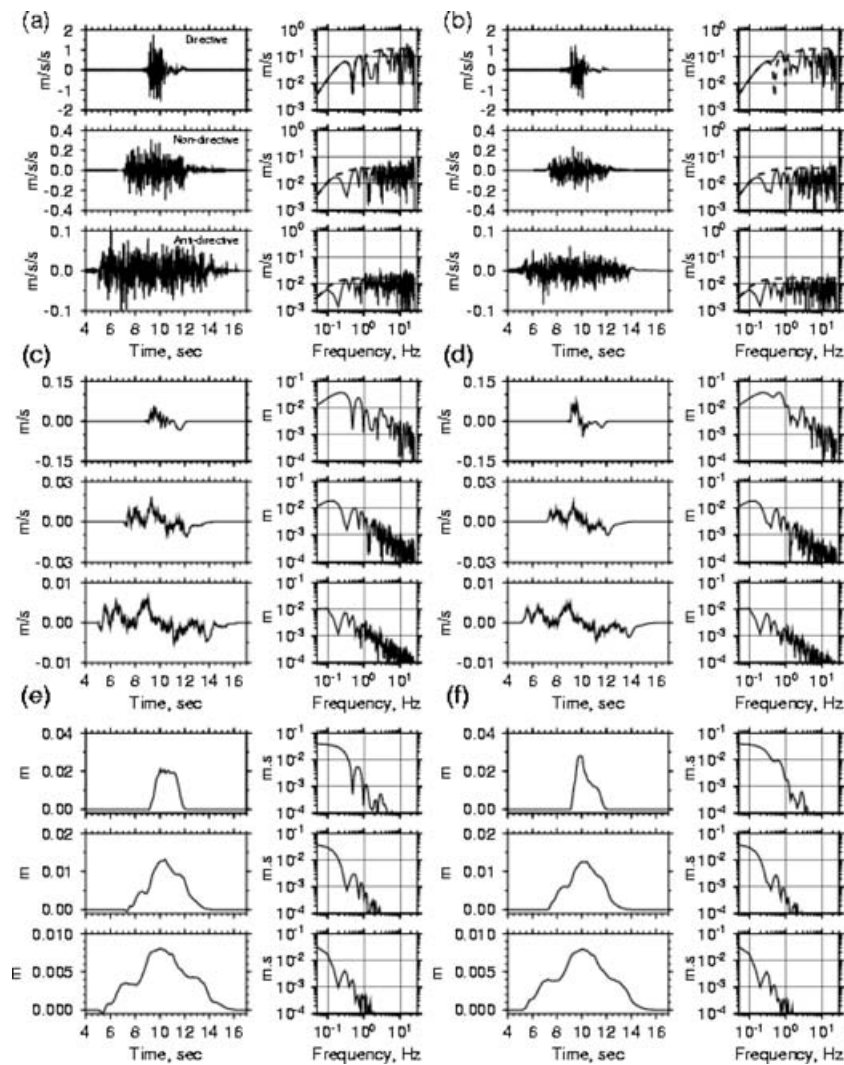


Figure 13. Same legend as Fig. 15 for τ_{max} equal to 2 s.

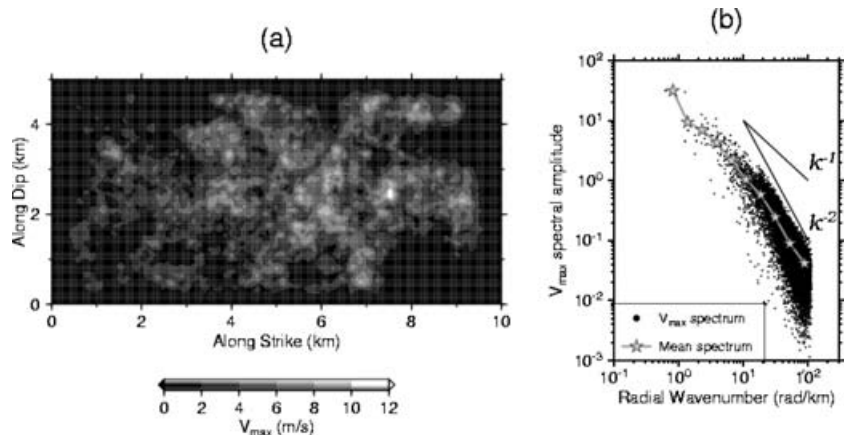


Figure 14. Peak-slip velocity, V_{max} , computed on the fault plane with the band of k approach. (a) Spatial distribution and (b) spectral amplitudes along the radial wavenumber.

modelling, we also attempt to validate our approach by comparing our estimates of PGA and PGV values with the ones predicted by empirical attenuation relationships. Synthetic accelerograms were computed for a M_w 6.0, earthquake on a vertical strike-slip fault

($10 \times 5 \text{ km}^2$) buried at 2.5 km (top of the fault). The stations are distributed radially in the near-fault region at distances ranging from 0 to 40 km (Fig. 15). The geological medium was modelled as a homogeneous half-space. Implicitly, we assume that at such short

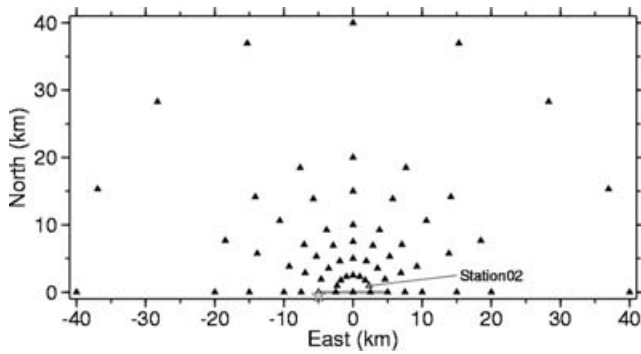


Figure 15. Source-station geometry used for modelling an M_w 6.0 earthquake. The fault plane corresponds to a vertical strike-slip buried at 2.5 km of depth.

distances to the fault, the strong ground motion is mainly controlled by the direct body waves. The complete wavefield Green's functions were computed up to 12 Hz using the code AXITRA (Coutant 1990) based on the Discrete Wave Number method (Bouchon & Aki 1977). Synthetic accelerograms were computed assuming a constant rupture velocity ($V_r/V_s = 0.8$). Several combinations of random slip

distributions (5) and hypocentral location along-strike (at -5 , -2.5 and 0 km) were used. The hypocentral depth was fixed at 5 km.

In Fig. 16, the ground velocity predicted at station 02 (Fig. 15) using the k^{-2} approach is compared with the one obtained using the band of k methodology. This example illustrates the importance of the SVF modelling. Indeed, the modelled S wave in the new methodology is more impulsive, due to the singularity at the rupture front of the SVFs. In terms of velocity spectrum, notice the disappearance of the spectral hole around 1 Hz, which was associated to the slip pulse.

Fig. 17 shows the horizontal PGA and PGV values estimated for all simulations as a function of the closest distance to the surface projection of the fault. Averaged curves (\pm the standard deviation) were estimated from the numerical data set. These results are compared to the values predicted by the empirical attenuation relationship defined by Sabetta & Pugliese (1987) from strong motion accelerograms recorded in Italy for shallow earthquakes. Our choice was motivated by the fact that these authors provided the attenuation coefficients for both PGA and PGV, which still remains uncommon. The mean PGA estimates are overall in good agreement with the empirical predictions (Fig. 17a). Nonetheless, our PGA estimates exhibit a large variability at all distances, larger than the empirical one in term of standard deviation. Concerning the PGV (Fig. 17b), our

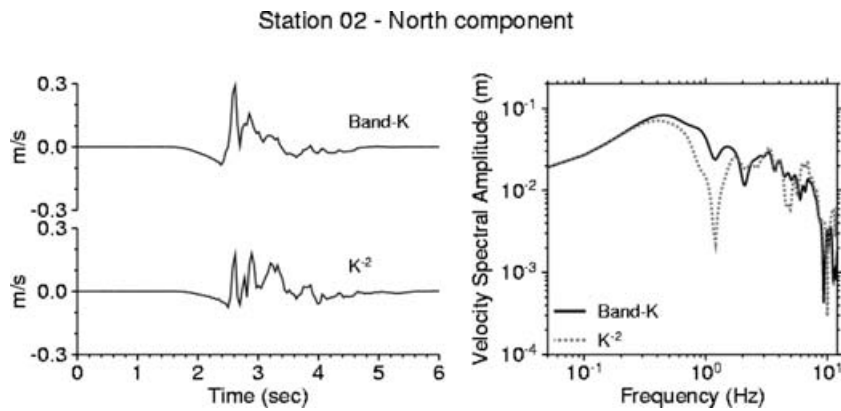


Figure 16. Comparison of ground-velocity time-series and the spectrum (north component) simulated at the station 02 ($R = 1$ km). Waveforms were modelled with the band of k (top) and standard k^{-2} (bottom) methodologies for a unilateral rupture scenario.

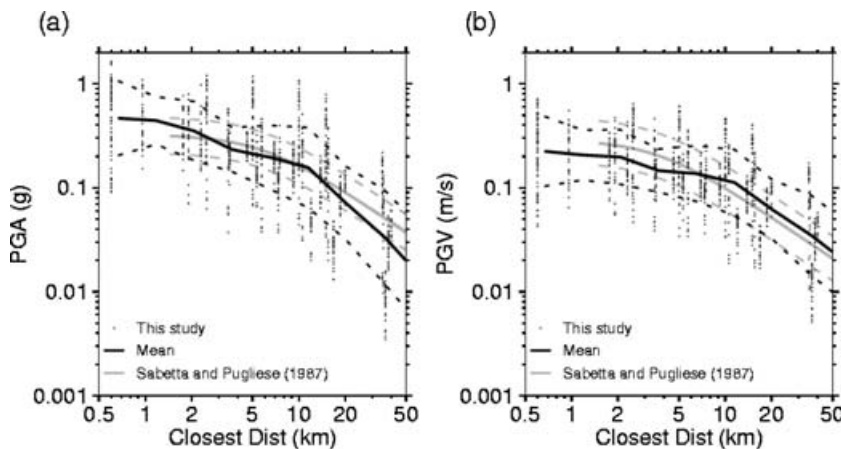


Figure 17. Comparison of simulated (circles) and empirical attenuation relationships (grey lines) for horizontal peak ground (a) acceleration, PGA and (b) velocity, PGV for a M_w 6.0 earthquake. In both cases dashed lines represent \pm the standard deviation. The predicted numerical values were computed using five random slip distributions and the band of k methodology for three rupture scenarios. Empirical attenuation relationships correspond to one derived by Sabetta & Pugliese (1987).

predictions are very similar on average to the empirical predictions, but are also associated to a larger standard deviation than the one of the empirical relationship. This large variability obtained both for the PGA and PGV is mainly related to the directivity effect. Indeed, many stations are located in the direction or the opposite direction of the rupture propagation, which may lead to overestimate the variability. Moreover, for a vertical strike-slip fault configuration, the effects of the radiation pattern and of the directivity are maximal for directive stations. Finally, the use of a half-space medium may also increase the variability estimate, given the fact that very coherent interferences are promoted in such a simple model.

7 CONCLUSIONS

In this paper, we have been investigating the stochastic kinematic k^{-2} source model proposed by Bernard *et al.* (1996), and in particular the SVF modelling which control the source radiation. The analysis we made revealed that the modelled SVFs are characterized on the fault plane by a large variability in space–time that can be related to the selected source model (heterogeneous slip and the scale dependent rise time). We have shown that the mean SVF solution is very different from the solutions proposed by dynamic modelling. Moreover, in the areas of weak slip, the SVFs are not realistic as they exhibit negative slip velocity values. When using a large rise time τ_{\max} , the proportion of fault area affected by unsatisfactory SVF modelling increases. The detailed analysis of the procedure followed to build the SVF led us to identify the Fourier decomposition as being responsible of the difficulties encountered. Indeed, in such an approach, the slip is decomposed into positive and negative contributions relatively to a low frequency distribution. Each contribution being set up with a scale dependent rise time, the resulting SVF can be locally negative, and very different from the typical impulsive dynamic solutions.

To counteract this difficulty, we proposed a new recombination scheme that leads to split the distribution into frequency-dependent positive contributions. Basically, it consists of defining a corrective term for each Fourier contribution, scaled to the product of p times the RMS of the slip computed by band of k . Several parametrical analyses have been made to characterize the effects of this correction on the far-field mean spectral shape, as well as on time-series. We have shown that adding a correction scaled to the RMS ($p = 1$) allows preserving the ω^2 spectral shape, and the C_d apparent directivity of the synthetic accelerograms, while the SVF are to the first order comparable to the dynamic SVF solutions proposed in the literature. Moreover, the holes in the acceleration spectrum predicted by the theoretical k^{-2} model are smoothed in the new procedure which is more satisfactory. As the correction is proportional to the RMS of the slip for each band of k , the procedure only depends on the slip distribution fluctuations, and not on the magnitude or on the fault dimensions. This new recombination scheme can thus be applied to events with a magnitude larger than the M6.0 tested in this study, and for any fault mechanisms.

Strong ground motions simulated in the near-fault region using the new band of k methodology yields to PGA and PGV predictions in good agreement with empirical prediction for mean value. The variability is however larger than the empirically predicted one mainly due to a combined effect of directivity and focal mechanism for a vertical strike-slip event.

The new recombination scheme, by decomposing the final slip into positive slip contributions, is more adapted to model the SVFs than a 2-D Fourier Transform analysis. Our proposed decomposition

can be seen as an attempt to link the standard k -square approach with composite source methods. Moreover, this study is only the first step for adding physical constraints in the kinematic modelling. Indeed, at this stage, the SVFs modelled with this kinematic approach are still singular at the rupture front arrival, whereas this singularity has been removed in dynamic rupture models by considering friction laws. Consequently, additional hypothesis on the kinematic rupture process must be done to handle this problem. For instance, other parameters must be taken in account, such as a variable rupture velocity, or a smooth radiation pattern at high frequency. Concerning the variable rupture velocity, even if it can be easily combined with the new approach proposed, the choice of a rupture velocity distribution on the fault plane must be made in order to obtain a dynamically consistent description of the parameters that define the rupture processes. This could be achieved using for instance a ‘pseudo-dynamic’ approach (Guatteri *et al.* 2004), which allows to link the rupture velocity to the slip through the fracture energy. Finally, further work must be done to compare our ground motion predictions with real records for large magnitude earthquakes for which the near-source effects become dominant.

ACKNOWLEDGMENTS

The authors are very grateful to the Editor Prof T. Dahm, to Dr P. Martin Mai and to an anonymous reviewer for their constructive comments, which help us to greatly improve the manuscript.

REFERENCES

- Abrahamson, N.A. & Silva, W.J., 1997. Empirical response spectral attenuation relations for shallow crustal earthquakes, *Seism. Res. Lett.*, **68**, 94–128.
- Aki, K., 1967. Scaling law of seismic spectrum, *J. Geophys. Res.*, **72**, 1217–1231.
- Aki, K. & Richards, P.G., 1980. *Quantitative Seismology: Theory and Methods*, Freeman, New York.
- Ambraseys N.N., Simpson, K.A. & Bommer, J.J., 1996. Prediction of horizontal response spectra in Europe, *Earthq. Eng. Struct. Dyn.*, **25**, 371–400.
- Anderson, J.G., 1997. Seismic energy and stress drop parameters for a composite source model, *Bull. Seism. Soc. Am.*, **87**, 85–96.
- Andrews, D.J., 1976. Rupture velocity of plane strain shear cracks, *J. Geophys. Res.*, **81**, 5679–5687.
- Andrews, D.J., 1980. A stochastic fault model, I. Static case, *J. Geophys. Res.*, **85**, 3867–3877.
- Andrews, D.J., 1981. A stochastic fault model II, Time-dependent case, *J. Geophys. Res.*, **86**, 10 821–10 834.
- Archuleta, R.J. & Hartzell, S.H., 1981. Effects of fault finiteness on near-source ground motion, *Bull. Seism. Soc. Am.*, **71**, 939–957.
- Baumont, D., Scotti, O., Courboux, F. & Melis, N., 2004. Complex kinematic rupture of the Mw 5.9, 1999 Athens earthquake as revealed by the joint inversion of regional seismological and SAR data, *Geophys. J. Int.*, **158**, 1078–1087, doi:10.1111/j.1365-246X.2004.02374.x.
- Beresnev, I. & Atkinson, G.M., 1997. Modeling Finite-Fault Radiation from ω^2 Spectrum, *Bull. Seism. Soc. Am.*, **87**, 67–84.
- Berge, C., 1997. Modélisation haute-fréquence des sources sismiques: application au risque sismique, *Ph. D thesis*, University of Paris VI.
- Berge-Thierry C., Cotton, F., Scotti, O., Griot-Pommer, D.A. & Fukushima, Y., 2003. New empirical response spectral attenuation laws for moderate European earthquakes, *J. Earth. Eng.*, **7**, 193–222.
- Berge-Thierry C., Bernard, P. & Herrero, A., 2001. Simulating strong ground motion with the “k-2” kinematic source model: an application to seismic hazard in the Erzincan Basin, Turkey, *Journal of Seismology*, **5**, 85–101.

- Berge-Thierry, C., Gariel, J.C. & Bernard, P., 1998. A very broad-band stochastic source model used for near source strong motion prediction, *Geophys. Res. Lett.*, **25**, 1063–1066.
- Berge-Thierry, C., Lussou, P., Hernandez, B., Cotton, F. & Gariel, J.C., 1999. Computation of the strong motions during the 1995 Hyogoken-Nambu earthquake, combining the k -square spectral source model and the discrete wavenumber technique, *The Effects of Surface Geology on Seismic Motion*, Proceeding of the Second International Symposium on the Effects of Surface Geology on Seismic Motion, Yokohama, Japan.
- Bernard, P. & Madariaga, R., 1984. A new asymptotic method for the modeling of near-field accelerograms, *Bull. Seism. Soc. Am.*, **74**, 539–559.
- Bernard, P., Herrero, A. & Berge, C., 1996. Modeling directivity of heterogeneous earthquake ruptures, *Bull. Seism. Soc. Am.*, **86**, 1149–1160.
- Boatwright, J., 1988. The seismic radiation from composite models of faulting, *Bull. Seism. Soc. Am.*, **78**, 489–508.
- Boore, D.M., 1983. Stochastic simulation of high frequency ground motion based on seismological models of the radiated spectra, *Bull. Seism. Soc. Am.*, **73**, 1865–1894.
- Boore, D.M., Joyner, W.B. & Fumal, T.E., 1997. Equations for estimating horizontal response spectra and peak acceleration from western North American earthquakes: a summary of recent work, *Seism. Res. Lett.*, **68**, 128–153.
- Bouchon, M. & Aki, K., 1977. Discrete wavenumber representation of seismic-sources wave fields, *Bull. Seism. Soc. Am.*, **67**, 259–277.
- Coutant, O., 1990. *Programme de Simulation Numérique AXITRA, Rapport LGIT*, Université Joseph Fourier, Grenoble, France.
- Dieterich, J.H., 1992. Earthquake nucleation on faults with rate- and state-dependent strength, *Tectonophysics*, **211**, 115–134.
- Frankel, A., 1991. High-frequency spectral falloff of earthquakes, fractal dimension of complex rupture, b value, and the scaling of strength on fault, *J. Geophys. Res.*, **96**, 6291–6302.
- Gallović, F., 2002. High frequency strong motion synthesis for $k-2$ rupture models, *Master thesis*. Dpto. of Geophys. Charles University, Prague.
- Gallović, F. & Brokešová, Y., 2004. On strong ground motion synthesis with $k-2$ slip distributions, *J. Seism.* **8**, 211–224.
- Guatteri, M., Mai, P.M., Beroza, G.C. & Boatwright, J., 2003. Strong ground motion prediction from stochastic-dynamic source models, *Bull. Seism. Soc. Am.*, **93**, 301–313.
- Guatteri, M., Mai, P.M. & Beroza, G.C., 2004. A pseudo-dynamic approximation to dynamic rupture models for strong ground motion prediction, *Bull. Seism. Soc. Am.*, **94**, 2051–2063.
- Herrero, A. & Bernard, P., 1994. A kinematic self-similar rupture process for earthquakes, *Bull. Seism. Soc. Am.*, **84**, 1216–1228.
- Horikawa, H., 2001. Earthquake doublet in Kagoshima, Japan: rupture of asperities in a stress shadow, *Bull. Seism. Soc. Am.*, **91**, 112–127.
- Ida, Y., 1972. Cohesive force across the tip of longitudinal-shear crack and Griffith's specific surface energy, *J. Geophys. Res.*, **77**, 3796–3805.
- Ide, S., 1999. Source process of the 1997 Yamaguchi, Japan, earthquake analyzed in different frequency bands, *Geophys. Res. Lett.*, **26**, 1973–1976.
- Inoue, T. & Miyatake, T., 1998. 3D Simulation of near-field strong ground motion based on dynamic modeling, *Bull. Seism. Soc. Am.*, **88**, 1445–1456.
- Irikura, K. & Kamae, K., 1994. Estimation of strong motion in broad band frequency band based on a seismic source scaling model and an empirical Green's functions technique, *Erice, Annali de Geophysicae*, **XXXVII**, 1721–1743.
- Joyner, W.B., 1991. Short Notes: directivity for nonuniform ruptures, *Bull. Seism. Soc. Am.*, **81**, 1391–1395.
- Kostrov, B.V., 1964. Self-similar problems of propagation of shear cracks, *J. Appl. Math. Mech.*, **28**, 1077–1087.
- Lavallée, D. & Archuleta, R.J., 2003. Stochastic modeling of spatial complexities for the 1979 Imperial Valley, California, earthquake, *Geophys. Res. Lett.*, **30**, 1245, doi:10.1029/2002GL015839.
- Mai, P.M. & Beroza, G.C., 2002. A spatial random field model to characterize complexity in earthquakes slip, *J. Geophys. Res.*, **107**, 2308, doi:10.1029/2001JB000588.
- Mai, P.M. & Beroza, G.C., 2003. A hybrid method for calculating near-source, broadband seismograms: application to strong motion prediction, *Phys. Earth Planet. Inter.*, **137**, 183–199.
- Miyakoshi, K., Kagawa, T., Sekiguchi, H., Iwata, T. & Irikura, K., 2000. Source characterization of inland earthquakes in Japan using source inversion results, *Proc. 12th World Conf. Earthq. Eng.*, Auckland, New-Zealand, 8 pp. (CDROM).
- Nakamura, H. & Miyatake, T., 2000. An approximate expression of slip velocity time function for simulation of near-field strong motion, *Zisin*, **53**, 1–9.
- Nielsen, S. & Madariaga, R., 2003. On the self-healing fracture mode, *Bull. Seism. Soc. Am.*, **93**, 2375–2388.
- Ohnaka, M. & Yamashita, T., 1989. A cohesive zone model for dynamic shear faulting based on experimentally inferred constitutive relation and strong-motion source parameters, *J. Geophys. Res.*, **94**, 4089–4104.
- Papageorgiou, A.S. & Aki, K., 1983. A specific barrier model or the quantitative description of inhomogeneous faulting and the prediction of strong motion, Part. I: description of model, *Bull. Seism. Soc. Am.*, **74**, 693–722.
- Sabetta, F. & Pugliese, A., 1987. Attenuation of peak horizontal acceleration and velocity from Italian strong-ground records, *Bull. Seism. Soc. Am.*, **77**, 1491–1513.
- Somerville, P.G. *et al.*, 1999. Characterizing crustal earthquakes slip models for the prediction of strong ground motion, *Seism. Res. Lett.*, **70**, 59–80.
- Tinti, E., Fukuyama, E., Piatanesi, A. & Cocco, M., 2005. A kinematic source-time function compatible with earthquake dynamics, *Bull. Seism. Soc. Am.*, **95**, 1211–1223.
- Tsai, C.-C.P., 1997. Slip, stress drop and ground motion of earthquakes: a view from the perspective of fractional Brownian motion, *Pure Appl. Geophys.*, **14**, 689–706.
- Tselentis, G.-A. & Zahradnik, J., 2000. The Athens earthquake of 7 September 1999, *Bull. Seism. Soc. Am.*, **90**, 1143–1160.
- Zeng, Y., Anderson, J.G. & Yu, G., 1994. A composite source model for computing realistic synthetic strong ground motions, *Geophys. Res. Lett.*, **21**, 725–728.

APPENDIX A

Mean SVF

The SVF modelled with the standard k^{-2} model can be expressed as follows:

$$\Delta \dot{u}(\xi, t) = \iint \Delta \tilde{u}(k) F[\tau(k), t] e^{ik\xi} dk,$$

where \mathbf{k} is the wavenumber, and ξ is point in the fault plane. In order to calculate the mean SVF, we assume that the origin of coordinates is located at the centre of a rectangular fault plane. Let us express the slip spectrum as $\Delta \tilde{u}(k) = |\Delta u(k)| e^{i\theta}$. The slip spectrum amplitude is constant, Δu_0 (mean slip), for $k < k_c$ and equal to $\Delta u_0 k_c^2 / k^2$ for $k > k_c$, where k_c is the corner radial wavenumber of the slip spectrum. The phase, θ , was taken to be uniformly random for $k > k_c$, and null for $k < k_c$. The k -dependent rise time $\tau(k)$ is equal to τ_{\max} for $k < k_0$ and $\tau_{\max} k_0 / k$ for $k > k_0$.

By taking the mean of the SVF at a given point ξ , by considering several realizations of stochastic slip, a straightforward calculus in polar coordinates yields a mean SVF consisting in a deterministic ($k < k_c$) and a stochastic ($k > k_c$) contributions:

$$\langle \Delta \dot{u}(\xi, t) \rangle = \int_0^{2\pi} \int_0^{k_c} \Delta u(k) e^{ik\xi \cos(\theta)} F[\tau(k), t] k dk d\theta + \int_0^{2\pi} \int_{k_c}^{k_{\max}} \Delta u(k) \langle e^{ik\xi \cos(\theta) + i\phi} \rangle F[\tau(k), t] k dk d\theta,$$

where k_{\max} is the maximum radial wavenumber. Assuming that the phase is uniformly random in the second term, the expected value of $\langle e^{ik\xi \cos(\theta) + i\phi} \rangle$ is equal to zero. We can write the expected SVF in

a simplified way as:

$$\langle \Delta \dot{u}(\xi, t) \rangle = \Delta u_0 F(\tau_{\max}, t) \int_0^{2\pi} \int_0^{k_c} e^{ik\xi \cos(\theta)} k dk d\theta,$$

integrating by θ first, using the property $\int e^{ik\xi \cos(\theta)} d\theta = 2\pi J_0(k\xi)$ and finally integrating by k , one finds the following deterministic solution for the mean SVF

$$\langle \Delta \dot{u}(\xi, t) \rangle = 2\pi \frac{\Delta u_0}{\tau_{\max}} k_c^2 \frac{J_1(k_c \xi)}{k_c \xi} H(\tau_{\max} - t) H(t),$$

where $J_0(\cdot)$, $J_1(\cdot)$ are Bessel functions and $H(\cdot)$ is the Heaviside time function.

Asymptotic behaviour of σ_{RMS} by band of k

The square of the standard deviation of slip grouped by band of k is computed as

$$\sigma_{\text{RMS}}^2[\Delta u_{B_n}(\xi)] = \int \int (\Delta u - \Delta \bar{u})^2 dx dy = \int \int \Delta u^2 dx dy,$$

where $\Delta \bar{u}$ is the mean slip estimated by band. This latter expression is obtained assuming that the mean slip by band is equal to zero. By using the Parseval's relationships we can compute the standard deviation in the wavenumber domain

$$\sigma_{\text{RMS}}^2(k) = \int \int \Delta u^2 dx dy = \int \int \Delta \tilde{u}^2(k_x, k_y) dk_x dk_y.$$

To calculate this expression, by construction of intervals of k (radial wavenumber), we evaluate this expression in the $B_n = [k_n, k_{n+1}]$ domain. We are looking for an asymptotic behaviour of σ_{RMS} , then we recall that the slip amplitude $\Delta \tilde{u}(k) \propto k^{-2}$, and by definition, $k_{n+1} = 2k_n$. Then a straightforward calculus yields

$$\sigma_{\text{RMS}}^2(k) \propto \int_{k_n}^{k_{n+1}} \frac{1}{k^4} k dk \propto \frac{1}{k_n^2},$$

by taking the square root, we obtain the standard deviation by band of k that is proportional to k_n^{-1}

$$\sigma_{\text{RMS}} \propto \frac{1}{k_n}.$$

The amplitude correction value, $\Delta u_c(k)$, can be estimated on average at first order as

$$\langle \Delta u_c(k) \rangle = \frac{\Delta u_{c, B_n}}{2^{2n}},$$

where $\Delta u_{c, B_n}$ is the slip correction of the band and 2^{2n} is the number of discrete wavenumber by band of k . The first wavenumber of each band is defined as $k_n = 2^n dk$, where all intervals are defined with a constant dk , then we can suppose that $k_n \propto 2^n$. We shown that slip correction by band of k is proportional to k_n^{-1} , then amplitude correction for each k is asymptotically proportional to

$$\langle \Delta u_c(k) \rangle \propto 1/k_n / 2^{2n} \propto 1/k_n / k_n^2 \propto 1/k_n^3.$$